Improved Thrust Restraint Design Considering Displacement of Pipe Bend and Joint Separation

Ohta, Yoko
Sawada, Yutaka
Kitada, Megumi
Kawabata, Toshinori

(Citation)
Journal of Pipeline Systems Engineering and Practice,14(2):04023006

(Issue Date)
2023-02-07

(Resource Type)
journal article

(Version)
Accepted Manuscript

Improved thrust restraint design considering displacement of pipe bend and joint separation

Yoko Ohta[1], Yutaka Sawada[2*], Megumi Kitada[3], and Toshinori Kawabata[4]

[1] Ph. D. Student, Graduate School of Agricultural Science, Kobe University, 1-1 Rokkodai-cho, Nada-ku, Kobe-shi, Hyogo 657-8501, Japan, y.ohta2020@gmail.com
[2] Associate Professor, Graduate School of Agricultural Science, Kobe University, 1-1 Rokkodai-cho, Nada-ku, Kobe-shi, Hyogo 657-8501, Japan, sawa@harbor.kobe-u.ac.jp
[3] Officer, Hyogo Prefectural Government, 5-10-1 Shimoyamate-dori, Chuo-ku, Kobe-shi, Hyogo 650-8567, Japan, Megumi_Kitada@pref.hyogo.lg.jp
[4] Professor, Graduate School of Agricultural Science, Kobe University, 1-1 Rokkodai-cho, Nada-ku, Kobe-shi, Hyogo 657-8501, Japan, kawabata@kobe-u.ac.jp

* Corresponding author

Abstract

The stability of pressure pipe bends is evaluated by the equilibrium between the thrust force and resistance forces in the current design, and the behavior of pipe bends is not considered. Force–displacement (F–D) relationships, which are used for predicting the displacement of pipe bends, include the performance of pipe joints in the design of pipe bends and shift the design method to a performance-based approach. However, F–D relationships have been proposed only under plane strain conditions. The behavior of pipe bends cannot be represented in two dimensions. Therefore, in this study, the prediction method of the F–D relationship for buried structures is extended to a three-dimensional condition to improve the design method of pipe bends with thrust restraint. Lateral loading experiments on thrust restraint, using rigid thrust blocks and flexible thrust restraints with geogrids and gravel, were conducted in dry sand to investigate the lateral behavior of rigid and flexible thrust restraints and to obtain F–D curves with different dimensions of thrust restraint. The experimental results revealed that the deformation of the flexible thrust restraint had little effect on the lateral resistance force if proper dimensions of the thrust restraints were determined. Using the experimental results, the F–D relationship was formulated based on a hyperbolic curve. The proposed equations were able to predict the resistance force relatively well at small lateral displacements. In addition to the formulation of the F–D relationship, a new design procedure considering the pipe displacement and performance of pipe joints was developed by combining the proposed F–D prediction method and the joint separation model proposed in previous studies.

Keywords: Force–displacement relationships; pressure pipeline; pipe bend; thrust restraint; joint

separation; design procedure

Introduction

Pipelines are essential facilities that support daily life; particularly, irrigation pipelines play an important role in transporting water from sources to fields. Irrigation pipelines must be designed to accommodate the diversity of pipe materials, diameter, and water pressures. For example, in Japan, seven kinds of materials are mainly used in irrigation pipes, with a diameter range between 100 mm and 3000 mm; moreover, pipes are applied water pressure ranging between 0.13 MPa and 1.33 MPa. In addition, there are many bends and branches in irrigation pipeline systems because these systems need to be laid on natural terrain which can be complex.

In the current design (e.g. Ministry of Agriculture, Forestry and Fisheries of Japan (MAFF) 2021; American Water Works Association (AWWA) 2013), the stability of the pressure-pipe bends is evaluated by the equilibrium between the thrust and resistance forces. This method is simple and useful, but lacks rationality because although the resistance force depends on the displacement of the pipe bends, the displacement of pipe bends is ignored in the current design method. Zarghamee et al. (2004) and Liu and Ortega (2021) proposed designs for continuous pipes and pipes with restraint joints, considering pipe–soil interaction. However, both designs have limitations because the aforementioned studies focused on pipes with mechanically restrained joints or continuous pipes; therefore, an improved design that considers the performance of ordinary pipe joints is required. Itani et al. (2016) and Shumaker et al. (2017) provided geometric relationships between the displacements of a pipe bend Y_{bend} and joint separation δ_j as shown in Fig. 1. The displacement of the pipe bend Y_{bend} owing to the thrust force can be predicted from force–displacement (F–D) relationships that have been established by experimental studies on anchor plates and pipes (Audibert and Nyman 1977; Das and Seely 1975; Ghaly 1997; Jung et al. 2016; Trautmann and O'Rourke 1985; Yimsiri et al. 2004 etc.). However, the Y_{bend}–δ_j and F–D relationships have been researched separately, and they have never been linked. The combination of Y_{bend}–δ_j and F–D relationships will help to incorporate the performance of pipe joints into the design of pipe bends and shift the design method to a performance–based approach. Although the F–D relationships of buried pipes have been proposed based on the experimental results under plane-strain conditions, Dickin and Leung (1983) and Ghaly (1997) pointed out from the results of pullout experiments on anchor plates that the width of anchor plates buried in sand

influenced the ultimate lateral resistance force and displacement. The F–D relationships proposed under plane-strain conditions cannot be used as the relationships of three–dimensional structures such as pipe bends. Hence, an F–D curve considering the three–dimensional (3D) condition is required for predicting the displacement of the pipe bend Y_{bend}.

When the resistance force against thrust force is insufficient, thrust restraint is required to prevent pipe failure, especially joint separation. A thrust block made of concrete is generally provided at the pipe bend to increase the resistance against the thrust force which consists of the passive earth pressure in the AWWA design (2013) or the passive earth pressure and the frictional force between the block and the surrounding ground in the MAFF design (2021). In active earthquake zones, such as Japan, thrust restraint without thrust blocks is often adopted in recent years because thrust blocks can cause pipe failure; this has been concluded from the investigations of earthquake damage of pipelines by Mohri et al. (1995) and Mohri et al. (2014). A geogrid and gravel have been studied to provide an aseismic thrust restraint since 2003 (Kawabata et al 2003). In this method, a pipe bend and the surrounding ground are wrapped in a geogrid, as shown in Fig. 2; the wrapped area is then backfilled with gravel. A geogrid, which is commonly used as a reinforcement of soil, increases the frictional resistance and unifies the wrapped area; whereas gravel increases the shear strength and the ability to dissipate pore water pressure. The effectiveness of gravel backfill as a thrust restraint under earthquake loading was evaluated using a centrifugal shaking table (Ohta et al. 2022). From experimental results, Ohta et al. (2018a) pointed out that the wrapped area by geogrids might be unified. Assuming the area wrapped by geogrids is completely unified, the wrapped area would behave as a single structure and the passive earth pressure and the frictional force would apply to the wrapped area in the same manner as a buried thrust block. However, the effectiveness of the method with geogrids is likely to be inferior to that of the thrust block when both methods use structures with same dimensions because the wrapped area with the geogrid is flexible compared to the rigid thrust block.

The aim of this study is to propose a new design method for thrust restraint that considers pipe displacement. Lateral loading experiments on thrust restraint were conducted to investigate the difference in lateral behavior of rigid and flexible thrust restraints and to obtain F–D curves under 3D conditions. Hyperbolic F–D relationships in 3D conditions were formulated based on the experimental results, and an outline of design methods considering pipe displacement was proposed with Y_{bend}–δ_f and F–D relationships.

Lateral loading experiments on rigid and flexible thrust restraints

Lateral loading experiments were conducted on the thrust block and thrust restraint with geogrids and gravel under 3D conditions to compare the lateral behavior of rigid and flexible restraints. In this paper, "3D conditions" means "not plane-strain conditions"; it does not refer to the effect of the shape of the pipe bends. A 1/9 scale experimental model was prepared based on the assumption that the prototype pipe has a diameter of 800 mm. Yamaguchi (2017) showed that pipelines with diameter between 500 and 1200 mm accounted for 41% of the length of irrigation pipelines in Japan. From the results of Yamaguchi (2017), a pipe with a diameter of 800 mm is commonly used for irrigation pipelines in Japan.

Outline of Experiments

The experiments in this study were conducted using the equipment shown in Fig. 3. The test equipment consisted of a test container, loading system, and displacement measurement system. The inner dimensions of the rigid test container were 1000 mm, 1100 mm, and 580 mm in width, length, and height, respectively. A hole was created in the wall at a height of 195 mm to allow a loading shaft of diameter 16 mm to penetrate the container wall. A loading system consisting of an electric actuator and a loading shaft was set outside the test container. The loading shaft was moved at a constant rate controlled by the electric actuator. A spherical seat was set between the shaft and model pipes or model boxes (explained in detail later); hence, that the pipes and boxes were able to move upward and downward. A load cell was placed between the loading shaft and the electric actuator to measure the resistance force acting on the model pipes and boxes. The frictional force between the loading shaft and the model ground was ignored in the experiments because the measured frictional force was too small to affect the experimental results. The displacement measurement system had two displacement transducers, pulleys, and a wire with a diameter of 0.8 mm. The right and left sides of the pipes or boxes were connected to the displacement transducers via a wire. The wire was passed through an aluminum tube in the model ground to decrease the friction between the wire and soil.

Dense and loose model ground was prepared using dry silica sand in the experiments. The particle size distribution is shown in Fig. 4. The dry unit weights of loose and dense silica sand were 13.4 kN/m^3 and 15.0 kN/m^3, respectively, which corresponded to a relative density of 30% and 80%, respectively. The maximum and minimum dry densities of silica sand were 12.5 kN/m^3 and 15.8 kN/m^3, respectively. The internal friction angles of dense and loose sand were 35.0 ° and 38.5 °, respectively, which were obtained by triaxial compression tests.

A PVC pipe was used as the model pipe. The outer diameter, thickness, and length of the pipe were 89 mm, 7 mm, and 300 mm, respectively. The boundary effect caused by the side walls of the container was negligible because the test container had sufficient width, more than three times the pipe width. Based on the calculation results, the model pipe was minimally deflected during the experiments. The unit weight of the model pipe was adjusted to 10 kN/m^3, with reference to the unit weight of the fiberglass reinforced plastic mortar (FRPM) pipe filled with water. To simplify the experimental conditions, a straight pipe was chosen even though the thrust force was generated at the pipe bend. Ohta et al. (2018b) conducted lateral loading experiments with model pipes with an outer diameter of 70 mm and bending angles of 30°, 60°, and 90°. The experimental results showed that the bending angle had minimal effect on the lateral resistance under the experimental conditions. Because the conditions of the experiments, such as the model scale in the present study, were similar to those of Ohta et al. (2018b), the influence of the bending angle on the lateral behavior of buried pipes appears to be insignificant in this experiment.

The photographs and dimensions of the flexible and rigid thrust restraint models are shown in Fig. 5. The flexible and rigid models had the same dimensions and weights. The value of *l'* as shown in Fig. 5 was changed into 1.0*D* (89 mm), 0.75*D* (67 mm) and 0.5*D* (45 mm), where *D* (mm) refers to the diameter of the model pipe. The width and height of the models were constant at 300 mm and 89 mm, respectively. Fig. 6 shows the procedure for preparing the flexible thrust restraint. As can be seen in Fig. 6 (a), the geogrid was connected to the model pipe using a jig that consisted of a screw, an L-shaped angle, and a small plate. The enclosed area surrounded by the geogrid was filled with gravel with a dry unit weight of 14.5 kN/m^3. The distribution and properties of the gravel are shown in Fig. 4. As can be seen in Fig. 6 (b), the ground on the passive side of the pipe was wrapped with a geogrid. The inside of the geogrid was filled with gravel. The model pipe and passive and active areas were wrapped with the geogrid (Fig. 6 (c)). The tensile stiffness of the geogrid with square openings of 10 × 10 mm was 77 kN/m, which is approximately 4% of the stiffness of the prototype geogrid used in the field test reported by Kawabata et al. (2010b). The results of the tensile tests on the prototype and model of the geogrid are shown in Fig. 7. The secant modulus at 2% strain obtained from Fig. 7 is regarded as the tensile stiffness in this study. Iai (1989) theoretically derived the similitude for 1G model tests on saturated soil–structure–fluid system. According to the study, the scaling factor for the longitudinal rigidity of buried structures could be represented as the 1.5th power of the geometrical scale factor. Following Iai's theory, the ideal scaling factor for the tensile stiffness of geogrids in the present study

can be obtained as follows:

$$\lambda_{ts} = (\lambda)^{1.5} = \left(D_m / D_p\right)^{1.5} = (89/800)^{1.5} = 0.037 \quad (1)$$

where λ and λ_{ts} are the scaling factors for the geometry and tensile stiffness, and D_m and D_p are the diameters of the model and prototype pipes, respectively. As described previously, the tensile stiffness of the model geogrid was 0.04 times the prototype. Thus, the model geogrid was suitable for reproducing the behavior of the prototype geogrid.

The rigid thrust restraint was simulated using wooden boxes as shown in Fig. 5(b). The wood plates had a thickness of 20 mm; this was sufficient to avoid deformation during the experiments. The spherical seat was set inside the box to push the boxes to the same position as the flexible thrust restraint models. The wire connected to the displacement gauge was placed on the active side of the box. The geogrid was fixed on the surface of the rigid thrust restraint models to receive the same frictional resistance as the flexible thrust restraint models.

The experimental procedure is as follows: The model ground was compacted into six layers. After two compacted layers with a total thickness of 150 mm, thrust restraint models or the model pipe were placed on the second layer. Four soil layers with a total thickness of 178 mm were compacted to fill the test models. After preparing the model ground, the test model was displaced laterally to 50 mm at a constant rate of 1.0 mm/s. The lateral resistance and displacement of the test models were measured during the experiments. After the experiments, the height of the ground surface was measured using a laser displacement sensor along the center line of the test container to investigate the deformation of the model ground. Table 1 summarizes the test conditions conducted in this study. The model type, dimension of *l'*, and ground density were changed, and a total of 14 tests were conducted.

Experimental results

Fig. 8 shows the variation in the lateral resistance force with the lateral displacement. In dense sand, the F–D curves have peaks at a displacement of approximately 5 mm. In loose sand, the resistance in all cases increases gradually. Similar characteristics of the F–D relationships have been shown in the experimental results of previous research on the behavior of buried pipelines under plane-strain condition (e.g., Trautmann and O'Rourke 1985). In some results of flexible thrust restraint, the development of the lateral resistance force was slightly delayed at the beginning of the lateral displacement. This may be due to voids remaining

in the area between the underside of the pipe and the bedding, called the haunch area. Compaction at the haunch area is difficult, as is well known, and even more so for small experimental models. In addition, the gravel used in this experiment was difficult to backfill in a narrow area because it contained no fine particles. Poorly established backfill at the haunch area may reduce the contact area between the pipe and backfill material and thus, decrease the increment of the lateral resistance at the beginning of the pipe displacement.

Comparing the results of flexible and rigid thrust restraints with the same dimensions, the resistance force of the flexible model is approximately the same as that of the rigid model when $l' = 0.75D$ and $0.5D$. Conversely, when $l' = 1.0D$, the resistance force in the flexible model was smaller than that in the rigid model. The resistance force in the flexible model with $l' = 1.0D$ hardly increased from $l' = 0.75D$ in both ground densities, even though the resistance force in the rigid models increased with an increase of dimensions. Fig. 9 shows the variations in the height of the ground surface at the center line of the test container obtained by the laser displacement sensor and shapes of the shear band appearing at the ground surface judged by sight. Only the results for dense sand are shown in Fig. 9 because the shear band in dense sand was easier to determine than that in loose sand. The failure zone in all cases was extended three-dimensionally. In addition, the failure zones in cases of flexible and rigid thrust restraints were larger than that of Case Pipe. When $l' = 0.75D$ and $0.5D$, there is little difference between the flexible and rigid models. These results correspond to the results that both lateral resistances are almost the same. The deformation of the flexible thrust restraint seems to have little effect on the lateral behavior. Conversely, when $l' = 1.0D$, the failure zone in the flexible model is smaller than that in the rigid model. Therefore, the resistance of the flexible model with $l' = 1.0D$ was smaller than that of the rigid model. Kawabata et al. (2007) conducted full-scale lateral loading experiments on a flexible thrust restraint only on the active side with two different dimensions. The results showed that the resistance force hardly increased with increase in length of the geogrid. They pointed out that there was an optimal dimension for the thrust restraint. A long geogrid is easy to extend owing to the characteristics of the geogrid; however, extending the geogrid seems to hinder unifying the wrapped area surrounded by the geogrid. Based on the experimental results, $l' = 0.75D$ is the optimal dimension under the experimental conditions for the flexible thrust restraint, and the influence of deformation in the wrapped area is minimal if the dimensions are less than $l' = 0.75D$.

Formulation of hyperbolic F–D relationships in 3D conditions

In this section, the F–D relationship for the thrust restraint method under 3D conditions is formulated based on a hyperbolic approximation in order to consider the displacement of the pipe bend in the design method. Because the experimental results revealed that the lateral behavior in the flexible thrust restraint was almost the same as that in the rigid thrust restraint, except for the results in $l' = 1.0D$, the formulation was conducted without distinguishing between flexible and rigid thrust restraints.

Procedure of formulation of F–D relationships

The F–D relationships in buried structures are often normalized by the ultimate resistance R_u and the ultimate displacement Y_u, where R_u (kN) is determined as the maximum resistance and Y_u (mm) is the displacement corresponding to R_u. According to Trautmann and O'Rourke (1985) and Jung et al. (2016), the normalized F–D relationships showed almost the same curve regardless of buried conditions such as dimensions of structures and depth of soil cover, and were often approximated by a rectangular hyperbola, written as follows:

$$R/R_u = (Y/Y_u)/\left[k_1 + k_2 (Y/Y_u)\right] \quad (2)$$

$$R' = Y'/k_1 + k_2 Y' \quad (3)$$

where R' and Y' are the resistance force and displacement normalized by R_u and Y_u, respectively, and k_1 and k_2 are coefficients. An inverse of Eq. (3) can be expressed as follows:

$$1/R' = k_1 \cdot 1/Y' + k_2 \quad (4)$$

The experimental results were substituted into Eq. (4), and the coefficients k_1 and k_2 are determined by linear approximation with the least squares method. F–D curves can be obtained by substituting the ultimate lateral resistance R_u and the ultimate lateral displacement Y_u into the normalized F–D relationships shown in Eq. (2). In other words, not only the normalized F–D relationships but also the ultimate lateral resistance R_u and the ultimate lateral displacement Y_u are required for predicting F–D relationships.

Identification of hyperbolic normalized F–D relationships

Fig. 10 shows the normalized F–D curves obtained from the experimental results. The resistance force and displacement were normalized by the ultimate resistance force and ultimate lateral displacement in each experimental result. The results for the rigid thrust restraint and the model pipe, shown in black in Fig. 10, indicate a general pattern regardless of the soil density, model dimensions, and model type. In contrast, the results of the flexible thrust restraint, shown in red in Fig. 10, are scattered, especially in case F-1.0*D*, which

is a flexible thrust restraint with l' = 1.0D buried in dense sand. This is owing to a small increment in the resistance force at the beginning of lateral loading, as described in Subsection 2.2. The broken line in Fig. 10 is the relationship proposed by Trautmann and O'Rourke (1985) based on the 2D experimental results. As can be seen in Fig. 10, the broken line did not match the experimental results. Thus, a normalized F–D relationship suitable for 3D conditions is proposed with the hyperbolic approximation described in the section "Procedure of Formulation of F-D Relationships". The obtained normalized F–D relationship is represented by the following equation:

$$R' = Y' / (0.096 + 0.903Y') \quad (5)$$

The values of k_1 (= 0.096) and k_2 (= 0.903) in Eq. (5) are the average values for each case, except for Case F-1.0D. The approximated curve is shown as a solid line on Fig. 10.

Prediction of the ultimate lateral resistance R_u

Duncan and Mokwa (2001), Al-Shayea (2006), Jadid et al. (2018), and Sharma et al. (2021) investigated the lateral resistance against a buried anchor block. In this study, the ultimate resistance is calculated from the equilibrium of the forces acting on a block, as illustrated in Fig. 11. Force equilibrium in the lateral direction is given by the following equation:

$$R_u = M(P_p - P_a) + P_t + 2P_s + P_b \quad (6)$$

where P_p is the passive resistance force (kN), P_a is the active resistance force (kN), P_t is the frictional force at the top of the block (kN), P_s is the frictional force at the side of the block (kN), P_b is the frictional force at the bottom of the block (kN), and M is the 3D effect factor proposed by Hansen (1966) based on the experimental results of Ovesen (1964). M was obtained by the following equation:

$$M = 1 + (K_p - K_a)^{0.67} \left\{ 1.1k_3^4 + 1.6k_4 / [1 + 5(b/h)] + 0.4(K_p - K_a) k_3^3 k_4^2 / [1 + 0.05(b/h)] \right\} \quad (7)$$

where

$$k_3 = 1 - h/(h + H) \quad (8)$$

$$k_4 = 1 \quad (9)$$

Coefficient k_4 enables the effect of the distance between structures to be considered. When a target is a single structure, as in the present study, 1 is substituted for k_4. Duncan and Mokwa (2001) indicated that the values of the calculated lateral resistance forces were relatively close to the measured values when the coefficient M was multiplied by the resistance force calculated from the 2D pressure theories such as Rankine, Coulomb

and log spiral theories. Each force in Eq. (6) is calculated as follows:

$$P_p = N_h hbH'\gamma_{soil} \quad (10)$$

$$P_a = K_a hbH'\gamma_{soil} \quad (11)$$

$$P_t = W_{soil} \tan\phi_{g-s} = blH\gamma_{soil} \tan\phi_{g-s} \quad (12)$$

$$P_s = hlH'\gamma_{soil} K_0 \tan\phi_{g-s} \quad (13)$$

$$P_b = \left[W_{block} + W_{soil}\right] \cdot \tan\phi_{g-s} \quad (14)$$

where N_h is the bearing capacity factor, h is the height of the block, b is the width of the block (m), l is the length of the block (m), H is the depth to the top of the block (m), H' is the depth to the center of the block (m), γ_{soil} is the unit weight of the surrounding soil (kN/m^3), ϕ_{g-s} is the friction angle between the soil and the geogrid (º), K_a is the coefficient of active earth pressure, K_0 is the coefficient of earth pressure at rest, W_{soil} is the weight of the soil above the block (kN), and W_{block} is the weight of block including the weights of pipe bend, water in the pipe, and gravel or concrete (kN). The bearing capacity factor N_h is determined by a chart, as shown in Fig. 12 which was based on Ovesen's theory (Ovesen 1964) and illustrated by Trautmann and O'Rounrke (1985).

In the buried pipe without thrust restraint, the ultimate resistance force R_u was calculated using Eq. (15), which is based on the equation proposed by Trautmann and O'Rourke (1985).

$$R_u = MN_h DB_{bend} H'\gamma_{soil} \quad (15)$$

where D is the pipe diameter (m) and B_{bend} is the projected width of the pipe bend (m). When determining the values of M and N_h for a buried pipe, b and h are replaced by B_{bend} and D, respectively. To confirm the validity of the calculated values of R_u obtained from Eqs. (6) and (15), a comparison between the calculated values and the experimental results is shown in Fig. 13. The internal frictional angle of soil was substituted for the friction angle between the geogrid and the surrounding soil, following the guidelines of the Geotextile Reinforced Soil Methods Promotion Committee (2013). The values of N_h in dense and loose sand were 6.75 and 5.45, respectively, as shown in Fig. 12. All the plots in Fig. 13 are near the straight line which is the diagonal line in Fig. 13. The calculated values obtained using Eqs. (6) and (15) were 83–106% of the experimental results. Thus, the ultimate resistance force of the thrust restraint and buried pipe can be predicted using the proposed equations.

Prediction of the ultimate lateral displacement Y_u

For buried pipes, Audibert and Nymann (1977) and Trautmann and O'Rourke (1985) presented equations for calculating the ultimate displacement according to soil cover, soil density, and pipe diameter. These equations were based on 2D experimental results and did not support the 3D condition. Therefore, new equations that consider 3D conditions are proposed in this study. In addition to the date set obtained in this study, the results of Ohta et al. (2018a) are used for formulation. Ohta et al. (2018a) conducted lateral loading experiments using a model pipe bend with a flexible thrust restraint. The test conditions are shown in Table 2 and Fig. 14. Fig. 15 shows the relationships between the ultimate displacement Y_u, the dimensions of blocks b, l, and h, and the depth to the center of the block H'. The results of the pipe without thrust restraint are also plotted in Fig. 15 with $b = 300$ mm, $l = D = 89$ mm, and $h = D = 89$ mm. For each soil density, the relationships between $Y_u/l/(H'/h)$ and b/l were almost linear. Y_u is represented by the following two equations, which are obtained from the linear approximation for each soil density.

$$Y_u = \left(0.006b + 0.006l\right) H'/h \quad \text{(for dense sand)} \quad (16)$$

$$Y_u = \left(0.039b + 0.006l\right) \cdot H'/h \quad \text{(for loose sand)} \quad (17)$$

Comparison between predicted and experimental F–D relationships

The validity of the predicted F–D curves obtained from the proposed equations is verified in this section. Fig. 16 shows the predicted and measured F–D relationships. In loose sand, the calculated curves almost fit the experimental results. In dense sand, the calculated value is close to the actual value at small displacements; however, at large displacements, it is significantly different from the measured value. This is because the calculated curves based on the hyperbolic approximation cannot predict the softening behavior of the resistance force. Although the proposed equations cannot reproduce the F–D relationship perfectly, this manually-calculated method is found to be useful in predicting the resistance force at small displacements, which is important for the stability of the pipe bend. Thus, the proposed equations can help predict the resistance of a pipe bend with or without thrust restraint considering the lateral displacement.

Proposal of a design method based on F–D relationships

The design procedure using the proposed equations is shown in this section. A specific method for considering pipe displacement in the design of thrust restraint is illustrated. An example of calculations using the proposed design procedure is provided in the latter half of this section.

Design chart for pipe bend

The proposed design procedure is illustrated in Fig. 17. The thrust force was calculated using the following well-known equation:

$$T = 2pA\sin\theta/2 \quad (18)$$

where T is the thrust force (kN), p is the internal water pressure (kPa), A is the cross-sectional area of the pipe (m^2), and θ is the bending angle of the pipe bend (º). To investigate the necessity of the thrust restraint, the F–D relationship of the pipe bend without thrust restraint is calculated first. The ultimate resistance R_{u1} was calculated using Eq. (15), and compared to the thrust force T. If $R_{u1} \leq T$, the pipe bend needs thrust restraint, and the thrust restraint is designed without calculating the ultimate lateral displacement Y_{u1}. If $R_{u1} > T$, the ultimate displacement, Y_{u1}, is calculated using Eqs. (16) or (17), and the calculated values of R_{u1} and Y_{u1} are substituted into Eq. (5) to obtain the F–D relationship: Y_{bend}, which is the pipe displacement when the value of the resistance force becomes equal to that of the thrust force T, is calculated by substituting T for R in the obtained F–D relationships. In this method, the stability of the pressure pipe bend is examined based on the allowable joint separation δ_{jallow}, and the allowable angular deflection ψ_{allow} for consideration of the behavior of the pipe bend. There are particular values of δ_{jallow} and ψ_{allow} for each product. The separation and deflection angle of a pipe joint can be obtained geometrically using the displacement of a pipe bend, Y_{bend}. As mentioned in the introduction, Itani et al. (2016) and Shumaker et al. (2017) provided equations for calculating the joint separation from the displacement of a pipe bend, based on the assumption of geometry, as shown in Fig. 1(a). The adjacent straight pipe in Fig. 1 was inserted fully in a straight alignment at the initial position. The separation δ_j and the angular deflection ψ are caused by the displacement of the pipe bend Y_{bend} and are calculated by the following equations:

$$\alpha = \sqrt{\left(L_{straight} + Y_{bend}\sin\theta/2\right)^2 + \left(Y_{bend}\cos\theta/2\right)^2} - L_{straight} \quad (19)$$

$$\psi = \tan^{-1}\left[Y_{bend}\cos\theta/2 \Big/ \left(L_{straight} + Y_{bend}\sin\theta/2\right)\right] \quad (20)$$

$$\delta_{jb} = D_{out}\sin\psi \quad (21)$$

$$\delta_{ja} = \alpha/2 - D_{out}/2 \cdot \sin\psi \quad (22)$$

$$\delta_j = \delta_{ja} + \delta_{jb} \quad (23)$$

where α is the joint separation at the pipe center (m), $L_{straight}$ is the length of the straight pipe (m), ψ is the angular deflection (º), δ_j is the total joint separation (m), δ_{ja} is the axial separation (m) and δ_{jb} is the separation

with angular movement (m). The value of separation δ_j can be negative depending on the combination of the values of D_{out}, $L_{straight}$, and ψ. When δ_j <0, there is no axial separation δ_{ja}, as shown in Fig. 1(b), and the separation δ_j needs to be recalculated using the following equation to avoid a negative value of δ_j.

$$\delta_j = \delta_{jb} = \alpha/2 + D_{out}/2 \cdot \sin\psi \quad (24)$$

Predicted δ_j and ψ need to satisfy the following equations.

$$\delta_{jallow} \geq \delta_j \quad (25)$$

$$\psi_{allow} \geq \psi \quad (26)$$

If δ_j or ψ exceeds the allowable value, thrust restraint is required for the pipe bend. After determining the dimensions of the thrust restraint, the ultimate resistance R_{u2} was calculated using Eq. (6), and compared to the thrust force T. If $R_{u2} \leq T$, the dimensions of the thrust restraint are reconsidered. If $R_{u2} > T$, the F–D relationship with thrust restraint is predicted using Eqs. (5), (6), (16), and (17). Y_{bend} is recalculated by substituting T into R for the F–D curve, and then δ_j and ψ are obtained using Eqs. (19)–(23). If the relationships shown in Eqs. (25) and (26) are not satisfied, the dimensions of the thrust restraint are reconsidered.

Calculation example using the proposed design method

A calculation example is presented to demonstrate the aforementioned procedure. Table 3 and Fig. 18 summarize the calculation conditions. The conditions for the pipe bends and joints were determined based on the actual values of an FRPM pipe with a diameter of 800 mm. The thrust force acting on the pipe bend is

$$T = 2 \cdot p \cdot A \cdot \sin(\theta/2) = 2 \times 1.0 \times 10^3 \cdot \left(800^2/4 \times \pi\right) \times \sin(30/2) \approx 260.2 \text{ (kN)} \quad (27)$$

The ultimate resistance against pipe bend R_{u1} is calculated as follows: N_h is determined as 5.45, as shown in Fig. 12.

$$K_a = (1 - \sin\phi_{soil})/(1 + \sin\phi_{soil}) = (1 - \sin 35)/(1 + \sin 35) \approx 0.27 \quad (28)$$

$$K_p = (1 + \sin\phi_{soil})/(1 - \sin\phi_{soil}) = (1 + \sin 35)/(1 - \sin 35) \approx 3.69 \quad (29)$$

$$M = 1 + \left(K_p - K_a\right)^{0.67} \left\{1.1k_3^4 + 1.6k_4 \Big/ \left[1 + 5\left(B_{pipe}/D_{out}\right)\right] + 0.4\left(K_p - K_a\right)k_3^3 k_4^2 \Big/ \left[1 + 0.05\left(B_{pipe}/D_{out}\right)\right]\right\}$$

$$= 1 + (3.69 - 0.27)^{0.67} \left[1.1 \times 0.5^4 + \frac{1.6 \times 1}{1 + 5 \times (1000/832)} + \frac{0.4 \times (3.69 - 0.27) \times 0.5^3 \times 1^2}{1 + 0.05(1000/832)}\right]$$

$$= 2.04 \quad (30)$$

$$R_{u1} = MN_h D_{out} B_{pipe} H' \gamma_{soil} = 2.04 \times 5.45 \times 832 \times 1000 \times 1248 \times 18.0 \times 10^{-9} \approx 208.2 \text{ (kN)} \quad (31)$$

The predicted ultimate resistance R_{u1} is smaller than the thrust force T. Thus, the pipe bend requires thrust restraint.

The dimensions of the thrust restraint are determined, as shown in Table 3 and Fig. 18. A flexible thrust restraint was selected in this example. The ultimate resistance against the pipe bend with thrust restraint R_{u2} was calculated as follows:

$$M = 1 + \left(K_p - K_a\right)^{0.67} \left\{1.1k_3^{\,4} + 1.6k_4 \Big/ \left[1 + 5\left(b/h\right)\right] + 0.4\left(K_p - K_a\right)k_3^{\,3}k_4^{\,2} \Big/ \left[1 + 0.05\left(b/h\right)\right]\right\}$$

$$= 1 + \left(3.69 - 0.27\right)^{0.67} \left[1.1 \times 0.5^4 + \frac{1.6 \times 1}{1 + 5 \times \left(1200/832\right)} + \frac{0.4 \times \left(3.69 - 0.27\right) \times 0.5^3 \times 1^2}{1 + 0.05\left(1200/832\right)}\right]$$

$$= 1.96 \quad (32)$$

$$K_0 = 1 - \sin\phi_{soil} = 1 - \sin\left(35°\right) = 0.43 \quad (33)$$

$$P_p = N_h hbH' \gamma_{soil} = 5.45 \times 832 \times 1200 \times 1248 \times 18.0 \times 10^{-9} = 122.2 \text{ (kN)} \quad (34)$$

$$P_a = K_a h_g b_g H' \gamma_{soil} = 0.27 \times 832 \times 1200 \times 1248 \times 18.0 \times 10^{-9} = 6.1 \text{(kN)} \quad (35)$$

$$P_t = W_{soil} \tan\phi_{g-s} = blH\gamma_{soil} \tan\phi_{g-s} = 1200 \times 1200 \times 832 \times 18.0 \times 10^{-9} \times \tan\left(35°\right)$$

$$= 15.1 \quad \text{(kN)} \quad (36)$$

$$P_s = hlH' \gamma_{soil} K_0 \tan\phi_{g-s} = 832 \times 1200 \times 1248 \times 18.0 \times 10^{-9} \times 0.43 \times \tan\left(35°\right) = 6.7 \text{ (kN)} \quad (37)$$

$$W_{water} = \left(D^2 \pi/4\right)\left[B_{bend} \Big/ \cos\left(\phi_{soil}/2\right)\right]\gamma_{water} = 800^2 \times \pi/4 \times 1000 \Big/ \cos\left(35/2°\right) \times 9.8 \times 10^{-9}$$

$$= 5.1 \quad \text{(kN)} \quad (38)$$

$$W_{gravel} = \left\{hbl - \left(D_{out}^{\,2} \pi/4\right)\left[b/\cos\left(\phi_{soil}/2\right)\right]\right\}\gamma_{gravel}$$

$$= \left\{832 \times 1200 \times 1200 - 832^2 \times \pi/4 \times 1200/\cos\left(35/2°\right)\right\} \times 10^{-9} \times 20.0 = 10.5 \text{ (kN)} \quad (39)$$

$$P_b = N_b \tan\phi_{g-s} = \left(W_{bend} + W_{water} + W_{gravel} + blH\gamma_{soil}\right) \cdot \tan\phi_{g-s}$$

$$= \left(1.2 + 5.1 + 10.5 + 1200 \times 1200 \times 832 \times 10^{-9} \times 18.0\right) \times \tan\left(35°\right) = 26.8 \text{ (kN)} \quad (40)$$

$$R_{u2} = M\left(P_p - P_a\right) + P_t + 2P_s + P_b = 1.96 \times \left(122.2 - 6.1\right) + 15.1 + 2 \times 6.7 + 26.8$$

$$= 283.5 \quad \text{(kN)} \quad (41)$$

The thrust restraint was confirmed to have the capacity to resist thrust force. Next, the ultimate lateral displacement Y_{u2} is calculated to obtain the F–D relationships.

$$Y_{u2} = \left(0.006b + 0.006l\right) H'/h = \left(0.006 \times 1200 + 0.006 \times 1200\right) \times 1248 / 832 = 23.0 \,(\text{mm}) \quad (42)$$

The F–D relationship can be expressed by substituting the calculated R_{u2} and Y_{u2} into Eq. (5).

$$R = R_{u2} Y / \left(0.096 Y_u + 0.903 Y\right) = 283.5 Y / \left(2.212 + 0.903 Y\right) \quad (43)$$

The pipe displacement Y_{bend} was calculated by substituting the thrust force T for R in Eq. (43).

$$T = 283.5 Y_{bend} / \left(2.212 + 0.903 Y_{bend}\right) \quad (44)$$

$$Y_{bend} = 2.212 T / \left(283.5 - 0.903 T\right) = \left(2.212 \times 260.2\right) / \left(283.5 - 0.903 \times 260.2\right)$$

$$= 11.9 \quad (\text{mm}) \quad (45)$$

The separation δ_j and angular deflection ψ are calculated using Eqs. (19)–(24).

$$\alpha = \sqrt{\left(L_{straight} + Y_{bend} \sin\theta/2\right)^2 + \left(Y_{bend} \cos\theta/2\right)^2} - L_{straight}$$

$$= \sqrt{\left(4000 + 11.9 \times \sin\left(30/2°\right)\right)^2 + \left(11.9 \times \cos\left(30/2°\right)\right)^2} - 4000 = 3.1 \,(\text{mm}) \quad (46)$$

$$\psi = \cos^{-1}\left[\left(L_{straight} + Y_{bend} \sin\theta/2\right) \Big/ \left(L_{straight} + \alpha\right)\right]$$

$$= \cos^{-1}\left\{\left[4000 + 11.9 \times \sin\left(30/2°\right)\right] \Big/ \left(4000 + 3.1\right)\right\} = 0.17 \quad (°) \quad (47)$$

$$\delta_{j2} = D_{out} \sin\psi = 832 \times \sin\left(0.17°\right) = 2.7 \,(\text{mm}) \quad (48)$$

$$\delta_{j1} = \alpha/2 - D_{out}/2 \cdot \sin\psi = 3.6/2 - 832/2 \times \sin\left(0.17°\right) = 0.3 \,(\text{mm}) \quad (49)$$

$$\delta_j = \delta_{j1} + \delta_{j2} = 0.3 + 2.7 = 3.0 \,(\text{mm}) \quad (50)$$

The calculated joint separation δ_j (=3.0 mm) and deflection angle ψ (=0.17º) were within the allowable values of δ_{jallow} (=128.0 mm) and ψ_{allow} (=2.0º), respectively. This result indicates that the thrust restraint is sufficient to maintain the stability of the pipe bend.

Conclusions

The aim of this study was to propose a new design method for buried pipe bends with thrust restraint considering lateral pipe displacement. The lateral loading experiments were conducted to investigate the lateral behavior of the flexible thrust restraint using geogrids and gravel compared to the rigid thrust restraint.

The F–D relationship of a pipe with thrust restraint was formulated under 3D conditions based on the experimental results. At the end of the study, a design procedure considering pipe displacement was proposed using the formulated equations. The main conclusions are summarized as follows.

1) The lateral behavior of the flexible thrust restraint was similar to that of the rigid thrust restraint. The deformation of the area wrapped by the geogrid had little effect on the lateral resistance. However, the lateral resistance did not increase when the dimensions of the wrapped area were extremely large because the integration effect of the geogrid was not fully realized.
2) The normalized F–D relationships showed almost the same curve regardless of the dimensions of the buried structure and soil densities. In addition, the normalized relationships based on the results of the 3D condition could be approximated by a hyperbola, as with those of previous studies of the 2D condition.
3) The ultimate lateral resistance force could be predicted by the proposed equations that were obtained from the equilibrium of forces considering the 3D effects.
4) The relationship between the ultimate lateral displacement and burial conditions was found to be linear.
5) By comparing the calculated values with the experimental results, the proposed equations were found to be able to predict the resistance force at a small lateral displacement. By combining the proposed equations with the joint separation model proposed in previous studies, the pipe displacement and performance of joints can be considered in the design of thrust restraints.

The equations proposed in this study were obtained under limited conditions. Careful consideration of the effect of scale, properties of geogrids and backfill material, etc. is required for the practical application of the proposed method. Further experimental and numerical studies could be conducted to resolve the limitations of the proposed equations. In future, the equations and design methods proposed could be improved so that they can be applied not only to irrigation but also to any pipeline system under pressure, such as water supply systems.

Data availability

Some or all data, models, or code that support the findings of this study are available from the corresponding author upon reasonable request.

Acknowledgement

This work was supported by JSPS KAKENHI Grant Numbers 20H00441 and 20J21213.

References

AWWA (American Water Works Association). 2013. *M45 Fiberglass Pipe Design*. 3rd ed. Denver: AWWA.

Audibert, J. M. E., and Nyman, K. J. 1977. "Soil restraint against horizontal motion of pipes." *J. Geotech. Eng. Div*. 103 (10): 1119–1142. https://doi.org/10.1061/AJGEB6.0000500.

Geotextile Reinforced Soil Methods Promotion Committee [In Japanese, translated by author]. 2013. *Design and Construction Manual for Reinforced Soil using Geotextiles* [In Japanese, translated by author], 2nd ed. Tokyo: Public Works Research Center.

Das, B. M., and Seely, G. R. 1975. "Load-displacement relationship for vertical anchor plates." *J. Geotech. Eng. Div*. 101(7): 711–715.

Dickin, E. A. and Leung, C. F. 1983. "Centrifugal model tests on vertical anchor plates." *J. Geotech. Eng*. 109(12): 1503–1525. https://doi.org/10.1061/(ASCE)0733-9410(1983)109:12(1503)

Duncan, J. M., and Mokwa, R. L. 2001. "Passive earth pressures: theories and tests." *J. Geotech. Geoenv. Eng*. 127 (3): 248–257. https://doi.org/10.1061/(ASCE)1090-0241(2001)127:3(248).

Ghaly, A. M. 1997. "Load-displacement prediction for horizontally loaded vertical plates." *J. Geotech. Geoenv. Eng*. 123 (1): 74–76. https://doi.org/10.1061/(ASCE)1090-0241(1997)123:1(74).

Hansen, J. B. 1966. "Resistance of a rectangular anchor slab." *Bull.* Danish Geotechnical Institute. 21: 12–13.

Iai, S. 1989. "Similitude for shaking table tests on soil-structure-fluid model in 1g gravitational field." *Soils Found*. 29 (1): 105–118. https://doi.org/10.3208/sandf1972.29.105.

Itani, Y., Fujita, N, Ariyoshi, M., Mohri, Y., and Kawabata, T. 2016. "Dynamic behavior of flexibly jointed pipeline with a bend in liquefied ground" [In Japanese]. *Trans. Jpn. Soc. Irrig. Drain. Rural Eng.* 301: I_1-I_8. https://doi.org/10.11408/jsidre.84.I_1.

Jadid, R., Abedin, M. Z., Shahriar, A. R., and Arif, M. Z. U. 2018. "Analytical model for pullout capacity of a vertical concrete anchor block embedded at shallow depth in cohesionless soil." *Int. J. Geomech*. 18(7): 06018017. https://doi.org/10.1061/(ASCE)GM.1943-5622.0001212.

Jung, J. K., O'Rourke, T. D., and Argyrou, C. 2016. "Multi-directional force–displacement response of underground pipe in sand." *Canad. Geotech. J.* 53 (11), 1763–1781. https://doi.org/10.1139/cgj-2016-

Kawabata, T., Sawada, Y., Izumi, A., Kashiwagi, A., Hanazawa, T., Okuno, S., and Suzuki, M. 2010. “Field verification test for buried bend with lightweight thrust restraint using geogrid.” In *Proc., 9th Int. Conf. Geosynth. Soc*, 1327–1332. Grajua: International Geosynthetics Society.

Kawabata, T., Sawada, Y., Ogushi, K., and Uchida, K., 2007. “Large scale tests of buried bend with lightweight thrust restraint method.” In *Proc. 17th Int. Soc. Offshore and Polar Eng. Conf*., 908-913. Lisbon: The International Society of Offshore and Polar Engineers.

Kawabata, T., Uchida, K., Tanaka, Y., Hirai, T., Saito, K., Sawada, Y., Nakase, H., Hirayama, T., and Imai, M. 2003. “Thrust protecting method for buried bend using the geosynthetics” [In Japanese]. *Geosynth. Eng. J*. 18: 215–220. https://doi.org/10.5030/jcigsjournal.18.215

Liu, M., and Ortega, R., 2021. “Thrust restraint of buried continuous pressure pipe considering pipe-soil interaction.” *J. Pipeline Syst. Eng. Pract*. 12 (4): 04021039. https://doi.org/10.1061/(ASCE)PS.1949-1204.0000577

MAFF (Ministry of Agriculture, Forestry and Fisheries of Japan). 2021. *Planning and design criteria of land improvement project (Pipeline)* [In Japanese, translated by author], Tokyo: The Japanese Society of Irrigation, Drainage and Rural Engineering.

Mohri, Y., Masukawa, S., Hori, T., and Ariyoshi, M. 2014. “Damage to agricultural facilities.” *Soils Found*. 54 (4): 588–607. https://doi.org/10.1016/j.sandf.2014.06.025

Mohri., Y., Yasunaka, M., and Tani, S., 1995. “Damage to buried pipeline due to liquefaction induced performance at the ground by the Hokkaido-Nansei Oki Earthquake in 1993.” In *Proc. 1st Int. Conf. Earthquake Geotech*. *Eng*., edited by K. Ishihara, 31–36. Tokyo: JGS.

Al-Shayea, N. 2006. “Pullout capacity of block anchor in unsaturated sand.” In *Proc. 4th Int. Conf. Unsaturated Soils*, 403-414. Arizona: ASCE. https://doi.org/10.1061/40802(189)29

Ohta, Y., Sawada, Y., Ariyoshi, M., Mohri, Y., and Kawabata, T. 2022. “Effects of gravel layer as thrust restraint for pipe bends subjected to earthquake loading.” *Int. J. Phys. Model*. *Geotech*. 22(2): 99–110. https://doi.org/10.1680/jphmg.20.00072

Ohta, Y., Sawada, Y., Ono, K., Kawamura, M., and Kawabata, T. 2018a. “Effects of shape dimensions of the lightweight thrust restraint method for buried pipe bend on additional lateral resistance.”[in Japanese] *Geosynth. Eng. J*. 33: 55–60. https://doi.org/10.5030/jcigsjournal.33.55

Ohta, Y., Sawada, Y., Ono, K., Ling, H. I., and Kawabata, T. 2018b. “Model experiments on influence of the bending angles on lateral resistance acting on buried pipe bends.” In *Proc. 28th Int. Ocean and Polar Eng. Conf.*, 589–593. Sapporo: The International Society of Offshore and Polar Engineers.

Ovesen, N. K. 1964. “Anchor Slabs, Calculation Methods, and Model Tests.” *Bull*. Danish Geotechnical Institute. 16: 5-39.

Sharma, A., Alzaylaie, M., Vandanapu, R., and Khalaf, K. 2021. “Numerical and analytical studies of 3D effects on pullout capacity of anchor blocks in granular compacted fill.” *Int. J. Geosynth. Ground Eng*. 7 (13): 1–8. https://doi.org/10.1007/s40891-021-00259-w.

Shumaker, S., Cashon, G., Cox, A., Conner, R., and Rajar, S. 2017. “Update to the improved approach for the design of thrust blocks in buried pipelines.” In *Proc. Pipelines 2017*, 586-596, Arizona: ASCE. https://doi.org/10.1061/9780784480878.053

Trautmann, C. H., and O’Rourke, T. D. 1985. “Lateral force-displacement response of buried pipe.” *J. Geotech. Eng.* 111 (9): 1077–1092. https://doi.org/10.1061/(ASCE)0733-9410(1985)111:9(1077)

Yamaguchi, Y. 2017. "A study on maintenance situation and risk management of irrigation pipeline." [in Japanese] *Water, Land and Environ. Eng*. 85 (10): 945–948.

Yimsiri, S., Soga, K., Yoshizaki, K., Dasari, G. R., and O’Rourke, T. D. 2004. “Lateral and upward soil-pipeline interactions in sand for deep embedment conditions.” *J. Geotech. Geoenv. Eng*. 130 (8), 830–842. https://doi.org/10.1061/(ASCE)1090-0241(2004)130:8(830)

Zarghamee, M. S., Eggers, D. W., Ojdrovic, R. P., and Valentine, D. P. 2004. “Thrust restraint design of concrete pressure pipe.” *J. Struct. Eng*. 130 (1), 95–107. https://doi.org/10.1061/(ASCE)0733-9445(2004)130:1(95)

Table 1 Test conditions in present study

Case	Model type	l' (mm)		Density
F-1.0D	Flexible thrust restraint (Pipe with geogrid and gravel)	1.0D	(= 89)	Dr = 80%, 30%
F-0.75D		0.75D	(= 67)	
F-0.5D		0.5D	(= 45)	
R-1.0D	Rigid thrust restraint (Wooden box)	1.0D	(= 89)	
R-0.75D		0.75D	(= 67)	
R-0.5D		0.5D	(= 45)	
Pipe	Model pipe	-	-	

Table 2 Summary of experimental condition reported by Ohta et al. (2018a)

Soil properties	Model pipe
Dry silica sand	Bend pipe
Unit weight of soil γ = 15.0 kN/m^3	Outer diameter D = 70 mm
Depth of soil cover H = 70, 140 mm	Bending angle θ = 30º

Table 3 Design parameters

Inner diameter of pipe	D	800 (mm)
Outer diameter of pipe	D_{out}	832 (mm)
Bending angle	θ	30.0 (º)
Width of pipe bend	B_{bend}	1000 (mm)
Length of straight pipe	$L_{straight}$	4000 (mm)
Allowable angular deflection	ψ_{allow}	2.0 (º)
Allowable total axial displacement	δ_{allow}	128 (mm)
Weight of pipe bend	W_{bend}	1.2 (kN)
Depth to pipe center	H'	1248 (mm)
Width of thrust restraint	b	1200 (mm)
Height of thrust restraint	h	832 (mm)
Length of thrust restraint	l	1200 (mm)
Unit weight of soil	γ_{soil}	18.0 (kN/m^3)
Unit weight of gravel	γ_{gravel}	20.0 (kN/m^3)
Unit weight of water	γ_{water}	9.8 (kN/m^3)
Water pressure	p	1.0 (MPa)
Internal friction angle	ϕ_{soil}	35.0 (º)
Friction angle between geogrid and soil	$\phi_{g\text{-}s}$	35.0 (º)

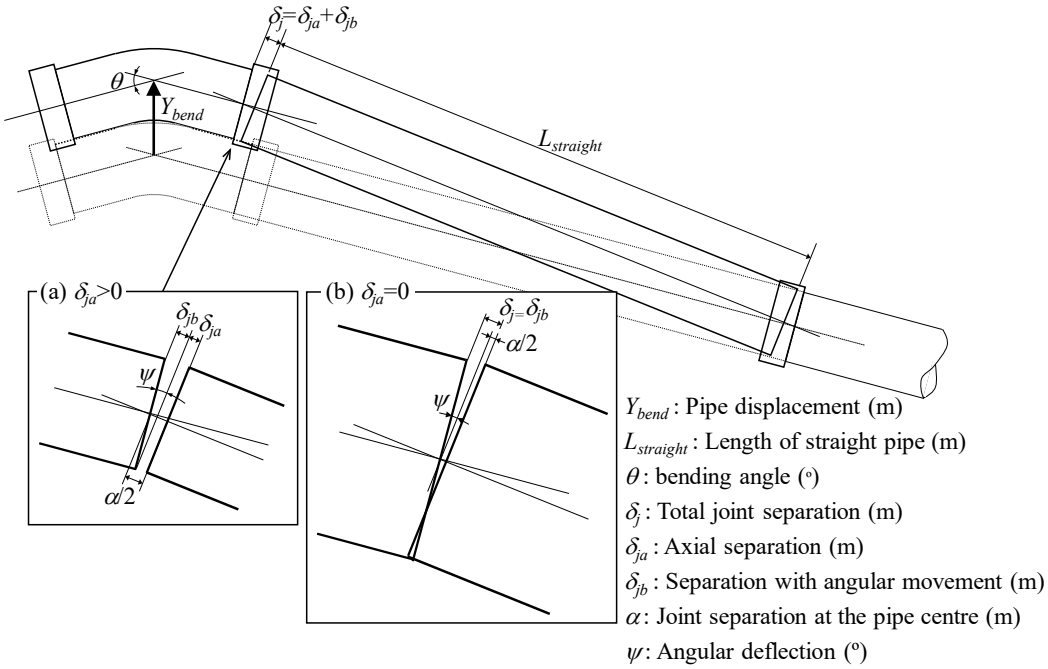

Fig. 1 Geometric relationships between pipe displacement Y and joint separation δ_j as proposed by Itani et al. (2016) and Shumaker et al. (2017)

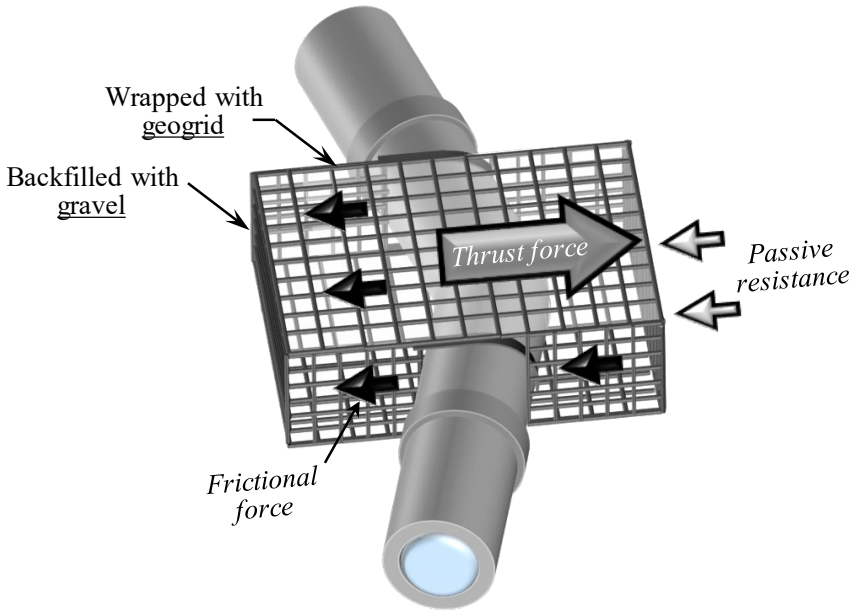

Fig. 2 Thrust restraint using geogrid and gravel

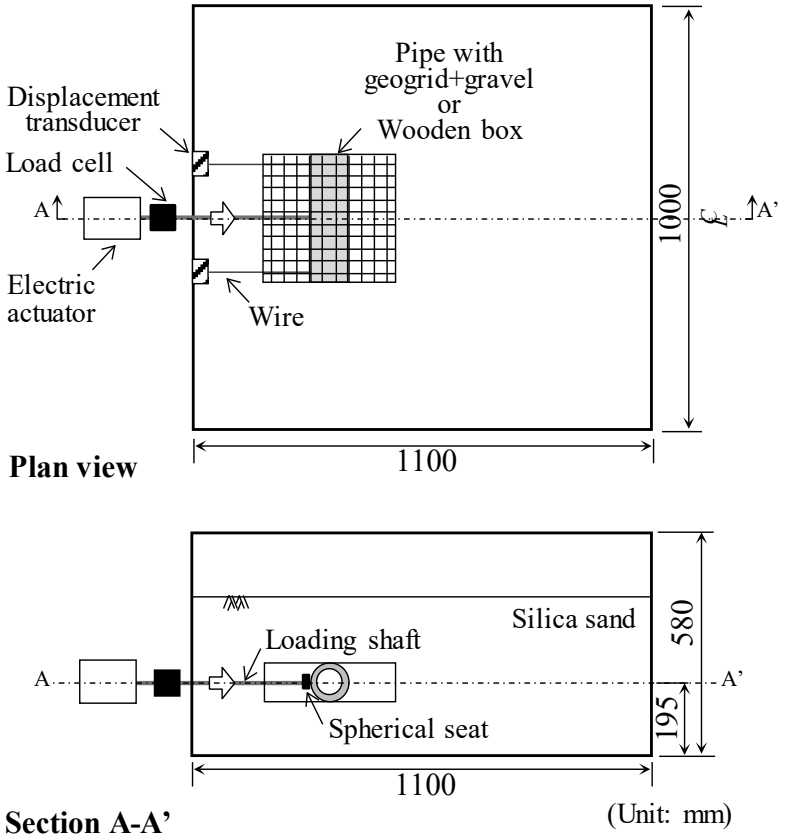

Fig. 3 Test equipment with flexible thrust restraint

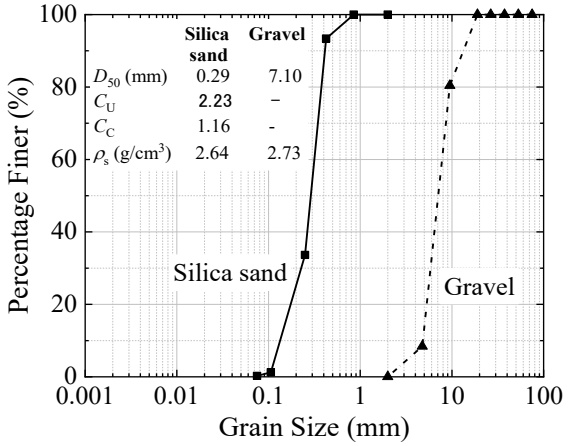

Fig. 4 Particle size distribution of silica sand and gravel

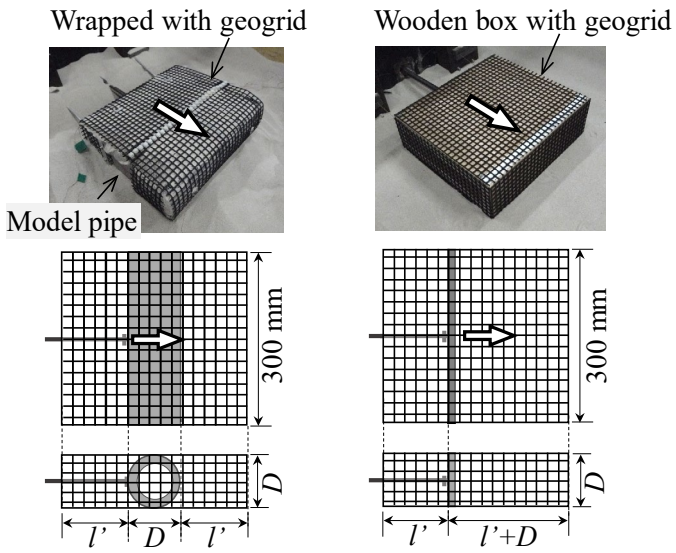

Fig. 5 Images and dimensions of flexible and rigid thrust restraint: (a) flexible thrust restraint, (b) rigid thrust restraint

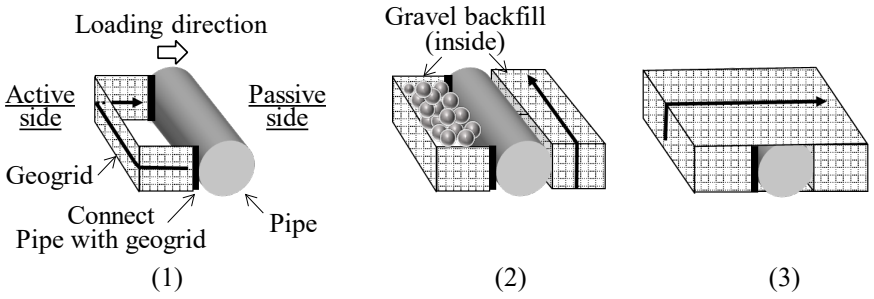

Fig. 6 Preparation of flexible thrust restraint

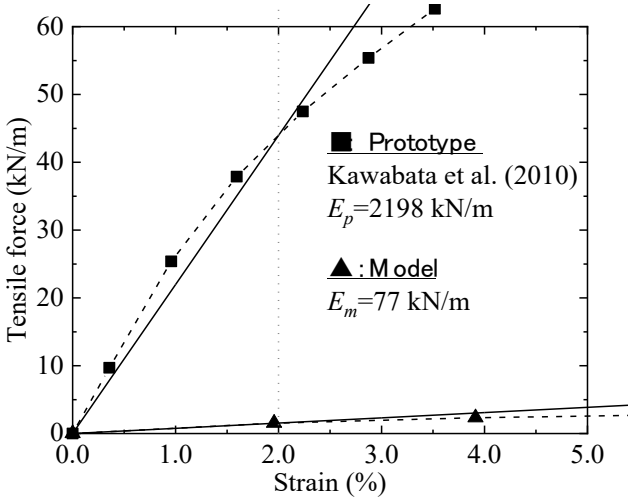

Fig. 7 Results of tensile tests on model and prototype geogrid

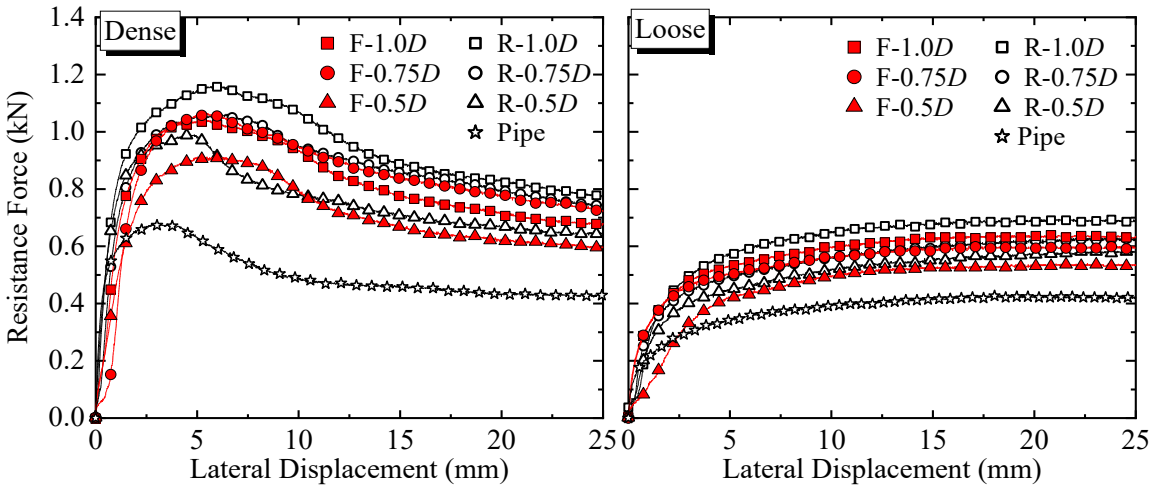

Fig. 8 Variation of lateral resistance with lateral displacement

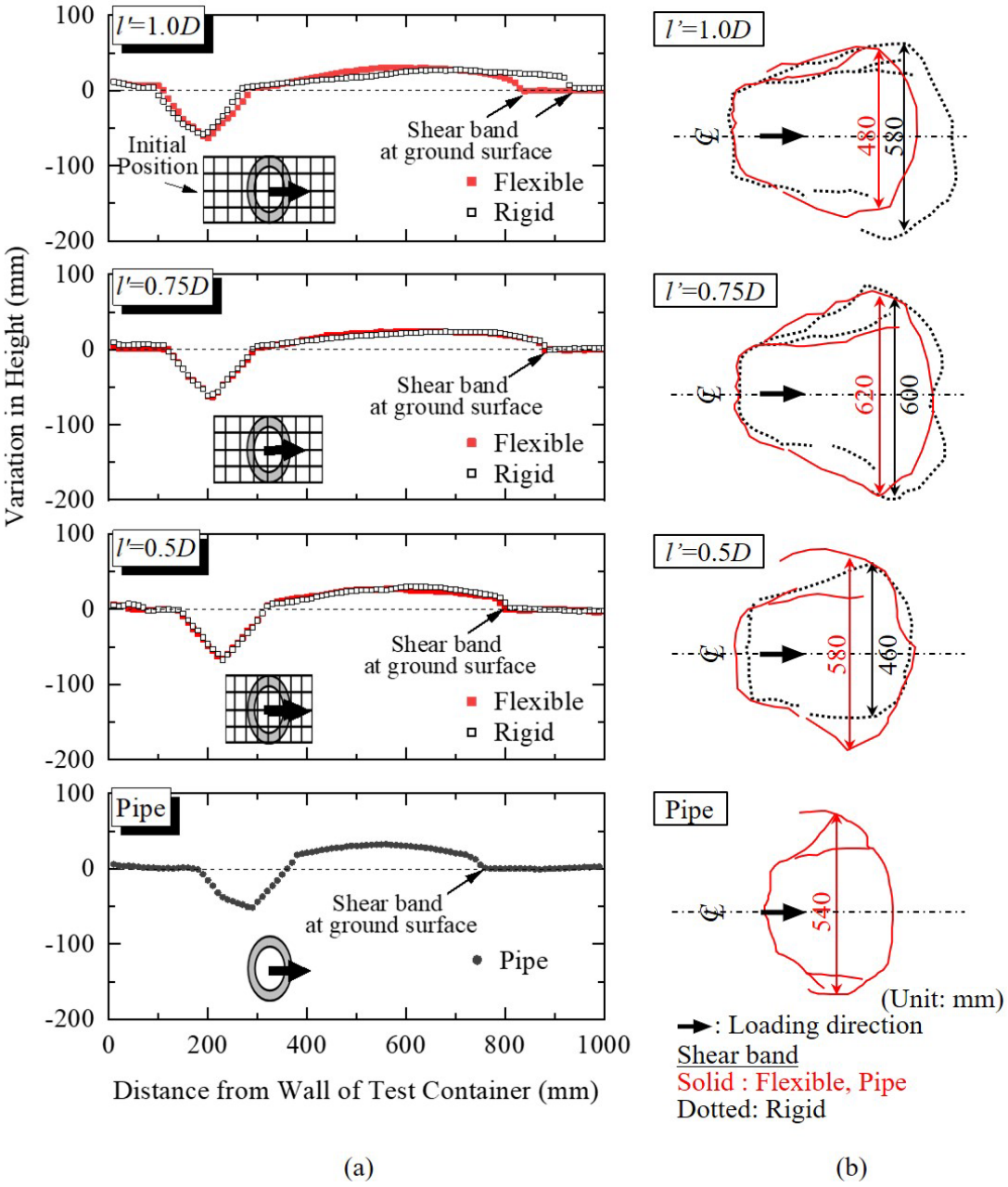

Fig. 9 Deformation of ground surface after experiments: (a) variations of height of ground surface at the center of the test container, (b) shear bands appeared at the ground surface

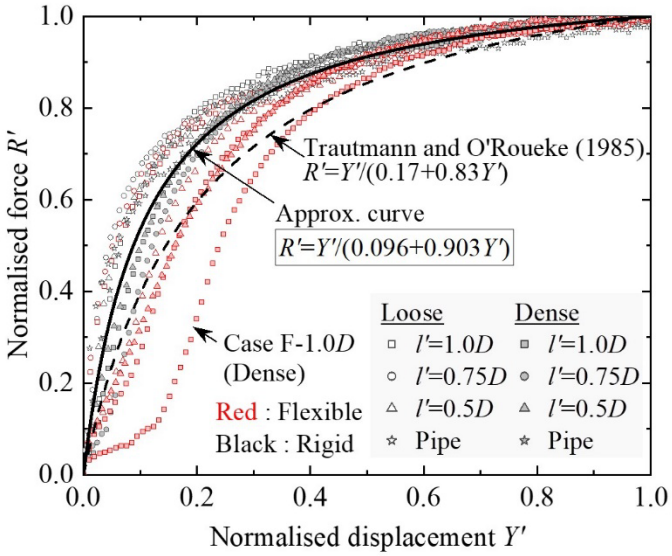

Fig. 10 Normalized force-displacement relationships of flexible and rigid thrust restraints and model pipes

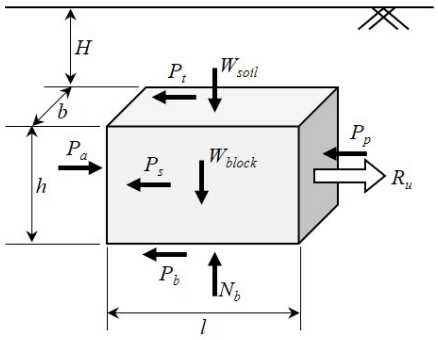

Fig. 11 External forces acting on buried block

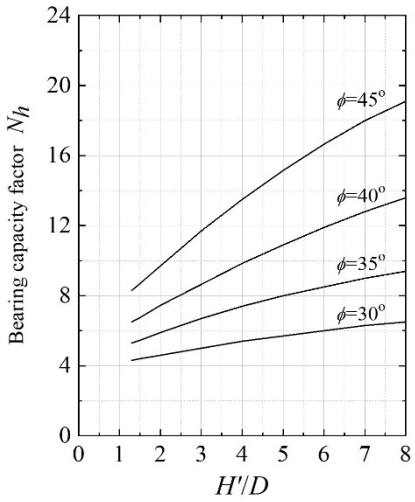

Fig. 12 Bearing capacity factors obtained by Ovesen's theory(Trautmann and O'Rourke, 1985; modified by author)

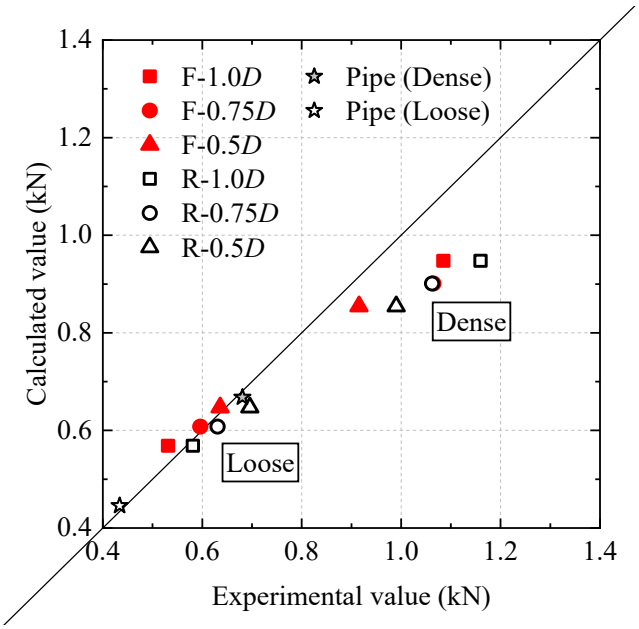

Fig. 13 Comparison between calculated and experimental value of lateral resistance

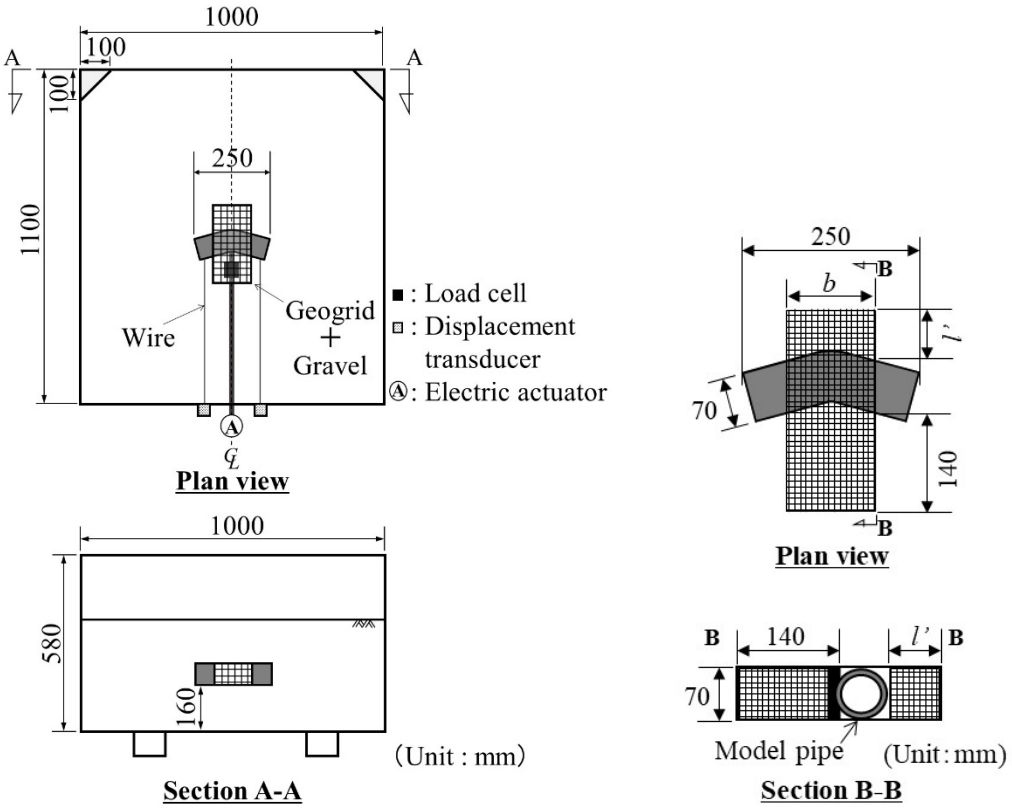

(a) Test container (b) Model pipe with thrust restraint

Fig. 14 Schematic diagram of experimental setup reported by Ohta et al. (2018a): (a) Test container, (b) Model pipe with thrust restraint (Ohta et al., 2018a; modified by authors)

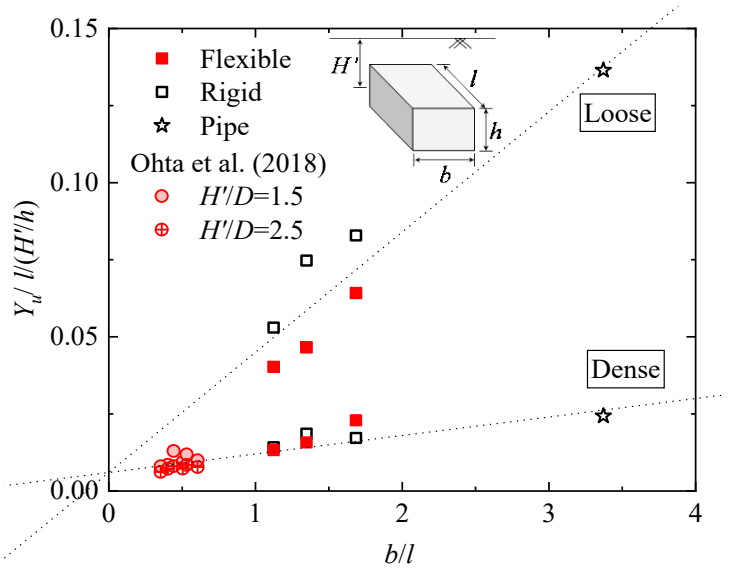

Fig. 15 Relationships between ultimate lateral displacement and buried conditions

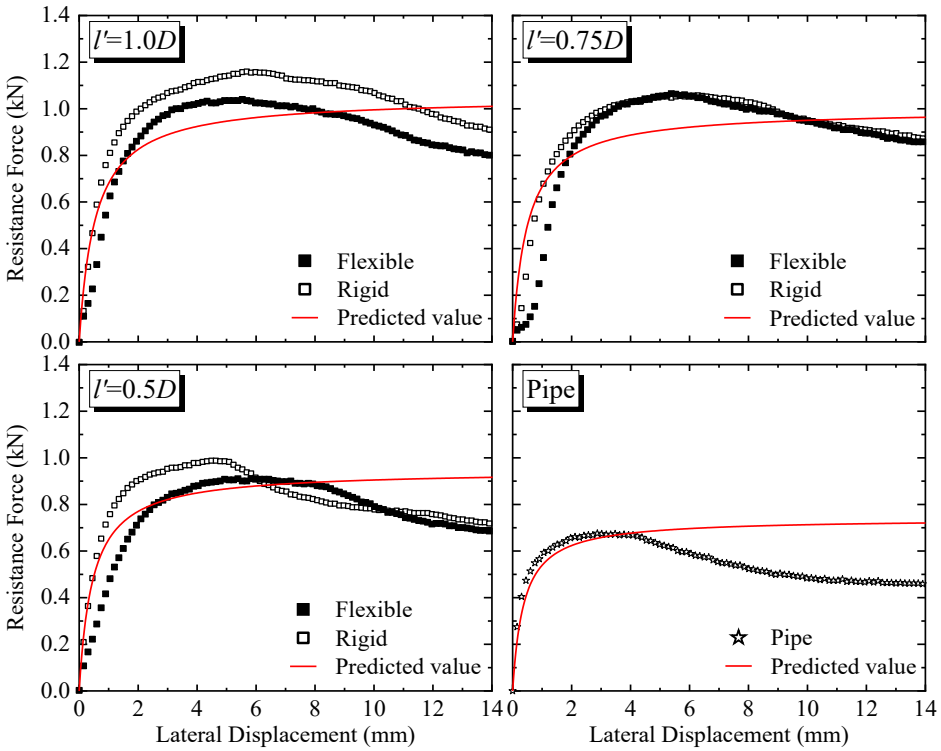

(a) Dense sand

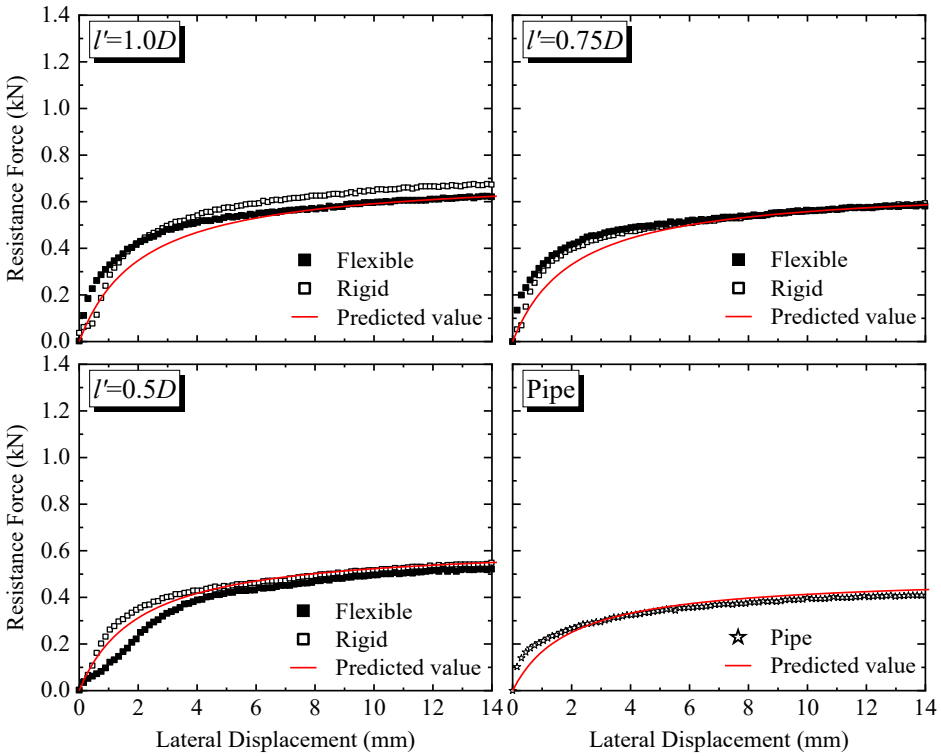

(b) Loose sand

Fig. 16 Predicted and measured F–D curves of flexible and rigid thrust restraint and buried pipe: (a) results in dense sand, (b) results in loose sand

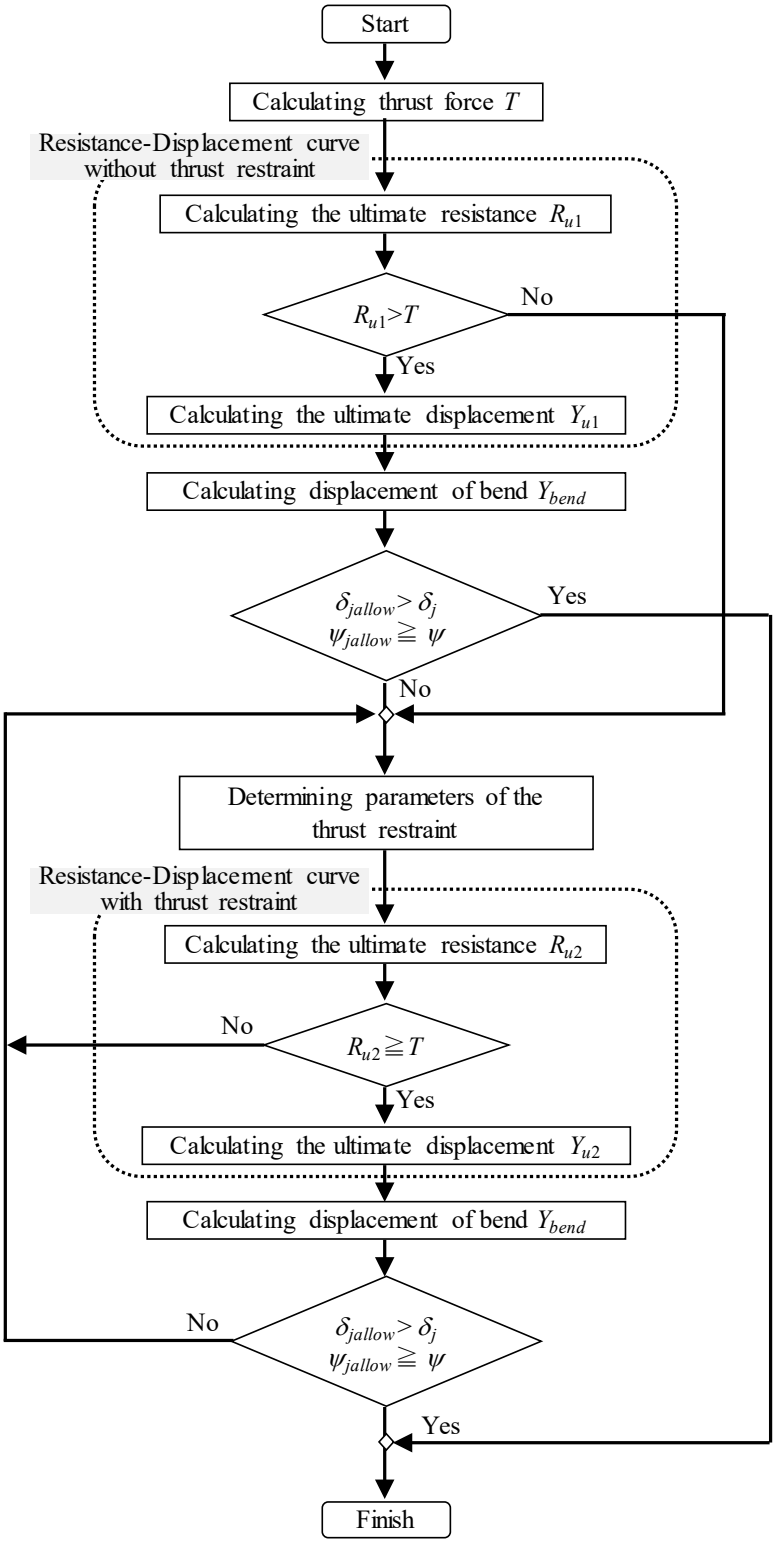

Fig. 17 Proposed design procedure considering pipe displacement

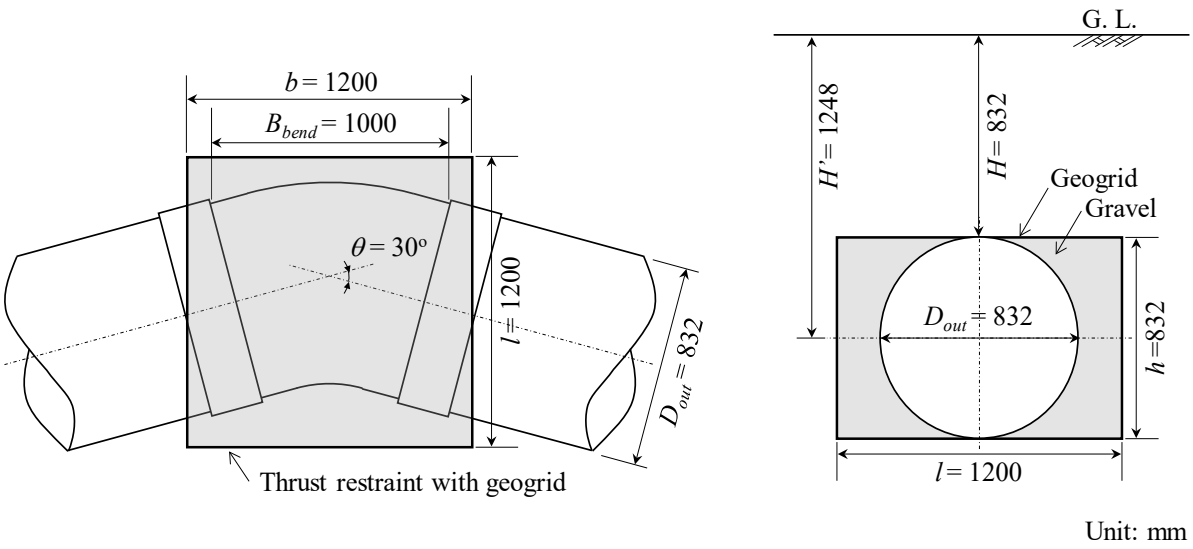

Fig. 18 Installation condition for target pipe bend